THE JOURNAL OF PHYSICAL CHEMISTRY C

Article

Cite This: J. Phys. Chem. C 2018, 122, 25595−25605

pubs.acs.org/JPCC

Molecular Dynamics Simulation of the Microscopic Sintering Process of CuO Nanograins Inside an Oxygen Carrier Particle

Haibo Zhao,* Jinfa Gui, Jie Cao, and Chaohe Zheng

State Key Laboratory of Coal Combustion, Huazhong University of Science and Technology, Wuhan, 430074, PR China

ABSTRACT: CuO-based materials as oxygen carrier (OC) always exhibit a weak sintering resistance at high temperature, which leads to a significant decrease of reactivity in chemical looping processes. Inert component is usually added to enhance the thermal stability and increase the specific surface area of OC particles. Detailed knowledge on the sintering mechanism of CuO nanograins within the bulk of OC particles and the interactions between active component and inert support materials is thus of considerable importance. In this study, molecular dynamics (MD) method was conducted to explore the fundamental understanding of CuO sintering mechanism and the effects of different support materials (TiO_2, ZrO_2, and SiO_2) on the sintering resistance of supported CuO nanograins. The sintering simulations of pure CuO nanograins show that CuO particle with smaller diameter or at higher temperature tends to be more amorphous. With respect to the sintering of two unsupported nanograins, it can be concluded that the neck growth during sintering is the joint effect of surface diffusion and grain boundary diffusion. Among these three composite OCs (CuO supported by TiO_2, ZrO_2, or SiO_2), CuO/ZrO_2 shows a better sintering resistance. The enlarged discrepancy on the surface area loss between different supported CuO nanograins with the rising of temperature emphasizes the importance of rational selection of support materials at high temperature.

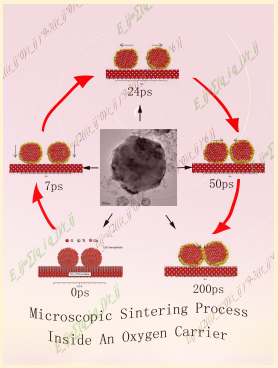

1. INTRODUCTION

It is well-believed that the CO_2 emission from fossil fuel combustion is a major factor for the aggravation of greenhouse effect. The reduction of CO_2 emission is in urgent need, and several CO_2 capture and storage (CCS) technologies have been developed to mitigate this emission within power generation processes.[1] Among these CCS technologies chemical-looping combustion (CLC) is a type of low-cost CO_2 capture technology and considered to be a promising low-carbon combustion/utilization technology of carbon-intensive fossil fuels.[2] CLC faces a tough challenge when utilizing solid fuels (e.g., coal) as the char gasification reaction is a rate-limiting step. A variant CLC process called chemical looping with oxygen uncoupling (CLOU)[3] was proposed to solve this problem. The key of CLOU is to identify high-performance oxygen carriers (OC) that are able to release gaseous O_2 at high temperature (800−1000 °C) and oxygen-deficient atmospheres. As O_2 is generated in fuel reactor (FR) during CLOU processes, it will help accelerate the char conversion, which eventually contributes to much higher CO_2 capture efficiency and combustion efficiency.

CuO is a superior candidate of CLOU oxygen carrier due to its high reactivity, high oxygen transport capacity, medium price, moderate environment impact, being exothermic for fuel combustion in FR, and suitable equilibrium partial pressure of oxygen at temperature of interest for combustion (800−1000 °C).[4,5] Despite of these favorable material properties, CuO with a quite low Tammann temperature (526 °C) suffers from a tendency toward sintering at CLOU temperature, which will lead to defluidization and low reactivity of the Cu-based OC particles. Usually, CuO is supported by inert materials to withstand high reaction temperatures. To date, a lot of materials including TiO_2, ZrO_2, SiO_2, Al_2O_3, $MgAl_2O_4$, and $CuAl_2O_4$[4,6,7] have been used as the support for CuO due to their thermally stability and high melting point. Various method (e.g., impregnation, sol−gel, mechanical mixing, spray drying) are adopted for the preparation of supported-CuO OC particles, and the preparation processes are almost involved in drying, granulation, calcination, grinding, and sieving.[8−10] How to choose appropriate support materials to enhance the sintering resistance becomes a challenge for the preparation of Cu-based OC.

The identification of high-performance OC based on the trial-and-error experiments is costly and time-consuming.[4,11] The Zener equation,[12] which is based on the idea that the driving pressure for first-phase grain growth (accompanying with particle sintering) due to the curvature of the grain boundary would be counteracted by a pinning pressure exerted by the second-phase particles (support materials) on the boundary, can be used to describe the active-component grain growth phenomenon as a function of the support material fraction, the type and size of the material, therefore helping rationalize the selection of inert materials.[13,14] However, the Zener pinning theory cannot provide any information about the actual process of grain growth, the growth rate or the size distribution of grains as a function of time,[15] let alone the morphology evolution and motion trail of particles during the high-temperature sintering processes. An intuitionistic guid-

Received: May 4, 2018
Revised: October 22, 2018
Published: October 22, 2018

DOI: 10.1021/acs.jpcc.8b04253
J. Phys. Chem. C 2018, 122, 25595−25605

ance on rational selection of inert supports may be provided by atomic-scale analyses about the interaction between active component and support, and a well understanding of the microcosmic sintering process is also of great benefit to the preparation of OC particles, including the optimization of particle formulation and dispersion.

Essentially, the sintering behavior of OC is dependent upon the microstructure, from the grain size to lattice arrangement. We[16] have used the density functional theory (DFT) to analyze the effect of support on the sintering resistance of supported-CuO particles, based on the analyses of adsorption energy and bond lengths. But it is still a nonintuitionistic criterion for the sintering resistance. Obviously, the sintering resistance is also associated with, at least, the grain size of active and inert components, the dispersion mode and mixing ratio between two components, which is hard to be handled by DFT since it is computationally infeasible to simulate the sintering process of nanograin system with too many atoms involved. Molecular dynamics (MD) simulation represents a powerful tool that can provide insights on the molecular mechanisms that drive and control the interactions at nanoscale. By solving the equation of motion for a system of particles, the real behavior of materials can be simulated under a specified temperature. The trajectory and physical movement of atoms, molecules, and nanoparticles (NPs) in the system can also be determined.

MD simulations have been successfully used to investigate the sintering performance of metal oxide at high temperature.[17−21] Schweigert et al.[17] studied the properties of SiO_2 clusters at temperatures from 1500 to 2800 K, and found that the diffusion coefficient plays a critical role in determining the primary particle size. Buesser et al.[19] studied the sintering of small (20 to 40 Å) rutile TiO_2 nanoparticles to complete coalescence, which showed that lower temperatures or larger primary particle diameters leads to slower sintering. Ahmed et al.[21] reported a detailed analysis of the nanoscale structure of CuO NPs as functions of size and temperature using MD simulations. It was found that the melting temperature is inversely proportional to the particle diameter, and the surface exhibits a distorted outer shell below the melting point. However, this study only paid attention to the melting feature of single CuO nanoparticle. In a realistic process, the sintering between different particles may lead to a more significant reduction of specific surface area, and the interaction between CuO and refractory material can inhibit the sintering effectively. Although some publications have investigated the sintering properties of composite particles (e.g., nickel/zirconia system[22,23]), to the best of our knowledge, the MD simulation on supported-CuO material has not been reported yet.

In this paper, a detailed description of the sintering characteristics of CuO nanograins (NGs) was investigated via MD simulations. The calculations started with the exploration of pure CuO nanograin sintering mechanism, where the effects of temperature and particle size were studied. Then, a cluster-slab model was used to clarify the role of different support materials in determining the sintering resistance of CuO at different temperatures.

2. COMPUTATIONAL DETAILS

The MD simulations were performed by the Discover package in Materials Studio. The constant-temperature, constant-volume canonical ensemble (*NVT*) was applied in the sintering simulations with a time step of 1.0 fs. The periodic boundary condition was adopted, and the cutoff radius was set as 0.95 nm, which was also adopted by some references.[24,25] The cutoff length is larger than the default Cutoff_Element values for "Fine" quality calculations (for O element, the default cutoff value for Fine quality calculations is 0.33 nm; 0.44 nm for Cu; 0.52 nm for Ti; 0.46 nm for Si; and 0.53 nm for Zr; see Materials Studio online help). To enable the canonical ensemble simulations, the Nose−Hoover temperature coupling[26] was selected to relax the atoms in the sintering system. Since the objective metal oxides in this study are various (CuO, TiO_2, ZrO_2, SiO_2), the force fields that are suitable for all these metal oxides are very limited. The COMPASS (condensed-phase optimized molecular potential for atomistic simulation studies) force field,[27] which is able to describe the interaction of many metal oxides, is an ideal choice for the calculations. In the COMPASS force field, a semi-ionic model[27] was used. Some involved parameters and physical properties of the COMPASS force field for the simulation of CuO,[28] TiO_2[28], and SiO_2[28−30] have been fully described in these references and well parametrized in Materials Studio. To the best of our knowledge, there is no such parameter description of ZrO_2 for the COMPASS force field from Materials Studio online help or any open reference. Materials Studio online help recommends that the semi-ionic model can be used for many metal oxides. In this work, we then used the COMPASS force field to simulate the ZrO_2 system. Factually, we only use the relevant simulation parameters and targeted physical properties in the Discover package of Materials Studio software. We did not define or modify these independence parameters and targeted physical properties in the MD simulations.

Atomic interactions in this force field model are divided into two types: directly contacted (bonded) interaction and indirectly contacted interaction. For the atoms that are directly bonded, the interaction energy is described by the Morse potential function and an electrostatic term:[28]

$$E_{ij} = \varepsilon\{\exp[-2\alpha(r_{ij} - r_{ij}^0)] - 2\exp[-\alpha(r_{ij} - r_{ij}^0)]\} \times f_s + (1 - f_s)\frac{C_6}{r_{ij}^6} + \frac{k_e q_i q_j}{r_{ij}} \quad (1)$$

where r_{ij} is the interatomic distance in Å, r_{ij}^0 is the equilibrium bond distance in Å, ε is trap depth energy in eV, C_6 is a parameter related to the bond energy, k_e is Coulomb's constant, the "width" of the potential is controlled by α in $Å^{-1}$, q is the partial charge of atom in e, and f_s is a continuous switching factor, which is defined as

$$f_s = \frac{1}{1 + \exp[20(r_{ij} - r_c)]} \quad (2)$$

where r_c is the radiation wavelength in Å. For the interactions between indirectly contacted atoms, the energy is described by the electrostatic term and VDW (van der Waals) term:

$$E_{ij} = \varepsilon\left[2\left(\left(\frac{r_{ij}^0}{r_{ij}}\right)^9 - 3\left(\frac{r_{ij}^0}{r_{ij}}\right)^6\right)\right] + \frac{k_e q_i q_j}{r_{ij}} \quad (3)$$

In this simulation, the "Ewald method" was adopted for the charge term[28,31] $k_e q_i q_j / r_{ij}$ of COMMPAS potential. On the basis of the help files of the Discover package in Materials Studio, we selected the summation method of "atom based" to

DOI: 10.1021/acs.jpcc.8b04253
J. Phys. Chem. C 2018, 122, 25595−25605

describe the van der Waals interactions, and adopted the Ewald method to evaluate Coulomb interactions with parameters of medium quality.

With respect to CuO (as an example), there are three types of atoms interaction: Cu−Cu, O−O, and Cu−O interactions. The interaction is divided into a bonded form and a nonbonded form, but only Cu−O bond interaction is formed in the bonded form, and the Morse potential function interaction is shown as Figure 1.

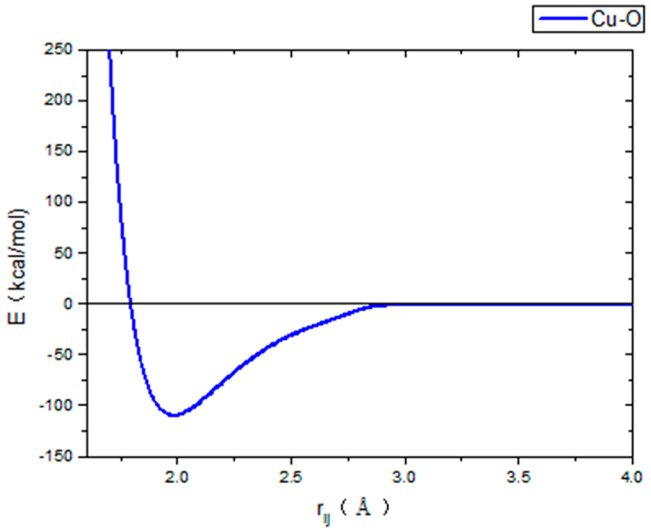

Figure 1. Morse potential.

The interaction potential exhibits a steady state of lowest energy, and it rises sharply as the bond distance decreases, then tends to zero as the bond distance becomes longer. For nonbonded interactions, as shown in Figure 2 and 3, the potential functions are divided into Lennard-Jones potential and Coulomb potential.

Comparatively speaking, the interaction of the bonded form is stronger than that of the nonbonded form. The nonbond interaction is very weak, but in its effective intercept radius space, the number of atoms that undergo nonbonding interactions is large and is applied to the atoms in superimposed form.

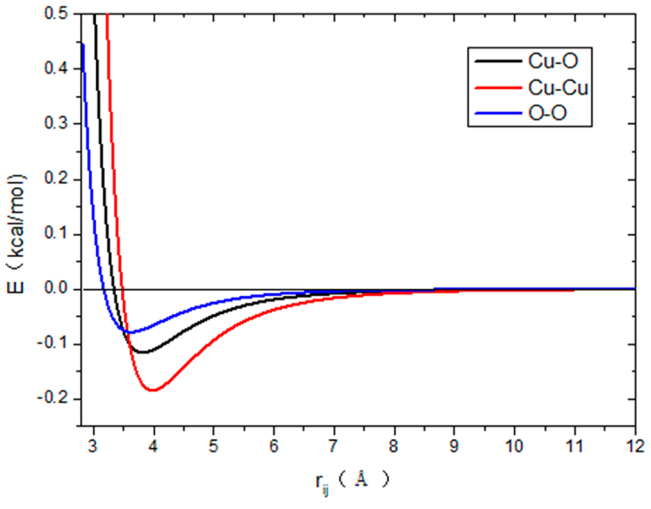

Figure 2. Lennard-Jones potential.

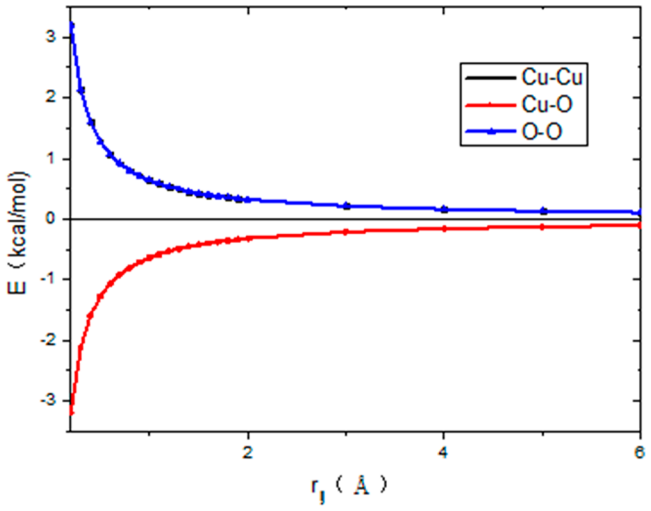

Figure 3. Coulombic potential.

In order to guarantee the computational accuracy of the MD simulation, the force field method and simulation parameters were tested. We first performed the geometry optimization calculation of CuO unit cell with these parameters described above, and the calculation results of Cu−O bond length at 0 K were given in Table 1. The MD result is close to the

Table 1. Cu−O Bond Length in the Optimized CuO Unit Cell

method	MD	DFT[32]	experiment[33]
length of Cu−O bond (Å)	1.98	1.95	1.96

experimental value[33] as well as the DFT result.[32] The high accuracy of Cu−O bond length is sufficient for the MD simulation of large amount of CuO molecules.

Then, we calculated the lattice parameters of the three inert supports of TiO_2, ZrO_2 and SiO_2 and compared then with the experimental data. As summarized in Table 2, the calculated results are very close to the experimental values,[34−36] indicating the validity of parameters setting in this work.

CuO is a monoclinic crystal and belongs to the C_2/C_1 space group. In this study, the CuO nanograins were assumed to be ideal spheres, and the initial CuO NGs with different diameters (30, 40, and 50 Å) in the sintering simulation were built by a spherical cut from the CuO super lattice, and excess atoms were removed from the surface. The constructed CuO cluster with diameter of 30 Å contains 1376 atoms, 3344 atoms for cluster diameter of 40 Å, and 6552 atoms for cluster diameter of 50 Å. Figure 4 presents the initial module of CuO cluster of 40 Å.

The stable low-index surface of support materials, TiO_2 (110), ZrO_2 (100), and SiO_2 (110), were selected as the calculated surface in this work, which were also cleaved from the bulk phase of TiO_2, ZrO_2 and SiO_2. The size of the TiO_2 (110), ZrO_2 (100), and SiO_2 (110) surface are 100 Å × 160 Å. The module of CuO cluster loaded on the surface of support material TiO_2 can be seen in Figure 5. In this work, the support materials of TiO_2, SiO_2 and ZrO_2 have been fixed, which was also similar to the simulation condition of ref 22. The module of CuO nanograins loaded on the fixed support surface (Figure 5) can be viewed as a simplification of a real oxygen carrier particle prepared by the impregnation method,

DOI: 10.1021/acs.jpcc.8b04253
J. Phys. Chem. C 2018, 122, 25595−25605

Table 2. Lattice parameters of TiO_2, ZrO_2 and SiO_2

support (group space)	calculation (this work)	experiment
TiO_2 ($P4_2/MNM$)	a = b = 4.48 Å; c = 3.00 Å; $\alpha = \beta = \gamma = 90°$	$a = b$ = 4.58 Å; c = 2.95 Å; $\alpha = \beta = \gamma = 90°$[34]
ZrO_2 ($P2_1/C$)	a = 5.17 Å; b = 5.11 Å; c = 5.32 Å; $\alpha = \gamma = 90°$; $\beta = 99°$	a = 5.15 Å; b = 5.21 Å; c = 5.32 Å; $\alpha = \gamma = 90°$; $\beta = 99°$[35]
SiO_2 ($P3_12_1$)	a = b = 4.89 Å; c = 5.36 Å; $\alpha = \beta = 90°$; $\gamma = 120°$	$a = b$ = 4.91 Å; c = 5.41 Å; $\alpha = \beta = 90°$; $\gamma = 120°$[36]

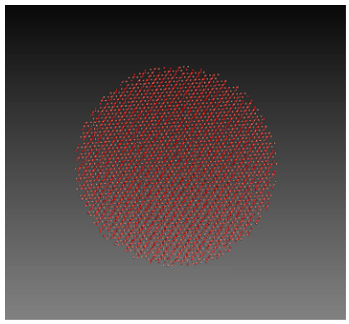

Figure 4. CuO cluster initial model.

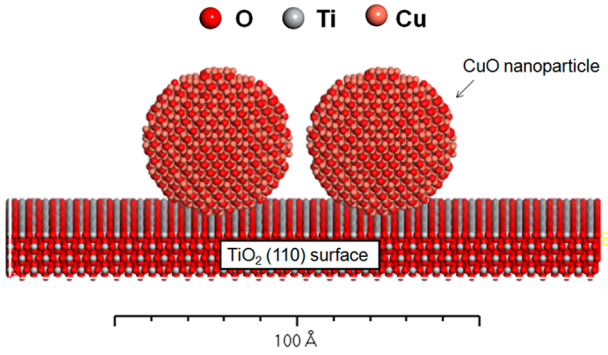

Figure 5. Atomic structure of CuO NGs and the support surface.

in which a small amount of active components (here CuO nanograins, usually with loading of <10 wt %) covers the bulk of support materials. Factually, this study established a fundamental methodology to illustrate sintering mechanism of CuO nanograins supported by three inert support materials. We mainly focused on the movement (or sintering) of CuO clusters, while the three support materials of TiO_2, SiO_2, and ZrO_2 have been fixed. It was speculated that the movement of support molecules (atoms) will be quite gentle in the MD simulations, and we then ignored the internal movement of support molecules (atoms).

In this work, the thicknesses of support materials, about 2 nm (nine-layer structure), referred to Xu et al.'s setting for simulating the sintering process of Ni nanoparticles in Ni/YSZ multinanoparticle system.[22] Because the support materials have been fixed, we therefore speculated that the thicknesses of support materials (about 2 nm) are feasible for modeling of bulky-particles. The residual stress and strain were not considered in the MD simulations. We also noted here that the thicknesses of support materials (ca. 2 nm) are larger than the cutoff length (0.95 nm).

3. RESULTS AND DISCUSSION

3.1. High-Temperature Sintering Characteristics of Pure CuO Grain. The structural properties of single CuO NG belong to vital and fundamental information to understand the CuO sintering behavior. A pure CuO particle with the diameter of 40 Å was put into a large cubic box (the length of side is 100 Å) and heated to the target temperature by Nose-Hoover temperature coupling for a total time of 1 ns. After this process, the radial distribution function (RDF) of CuO NG was counted to examine the structure features. The result is shown in Figure 6a.

Figure 6a shows that the RDF exhibits distinct characteristic peaks at 973, 1173, and 1373 K, and these significant peaks were all observed in the RDF curves at three different temperatures, which indicates that the CuO particles in high temperatures will still maintain a relative regular crystal lattice arrangement. The first strongest peak appears in the distance of 1.99 Å for all the three temperatures, corresponding to the Cu−O bond length in central position, which is very close to the ideal bond length of CuO crystal (1.95 Å). In addition, it also can be found that the RDF curves at higher temperatures tend to be slightly flatter, indicating the high-temperature

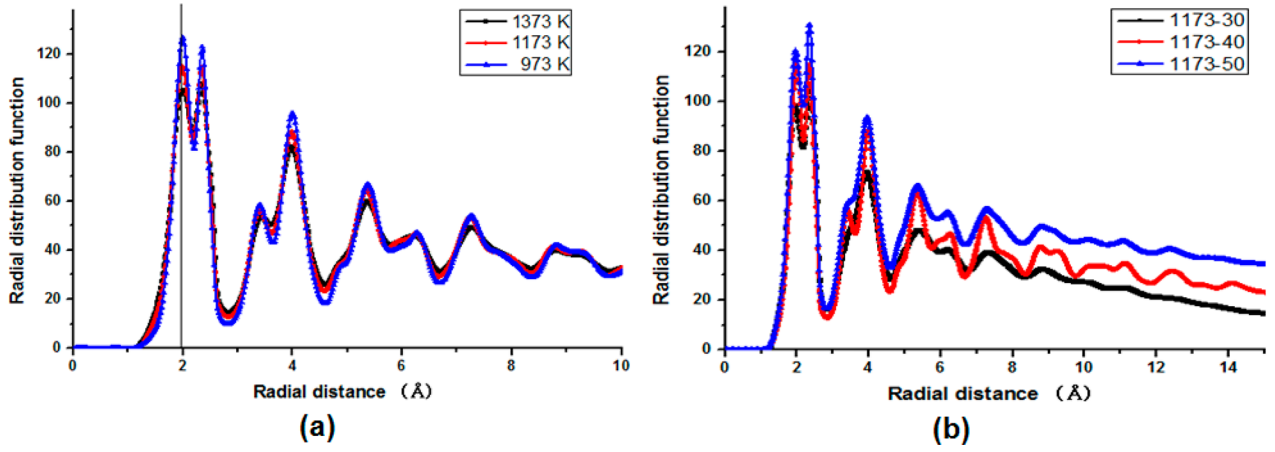

Figure 6. (a) RDF of 40 Å CuO NG at temperature of 973, 1173, and 1373 K. (b) RDF of CuO NG with diameters ranging from 30 to 50 Å at 1173 K.

DOI: 10.1021/acs.jpcc.8b04253
J. Phys. Chem. C 2018, 122, 25595−25605

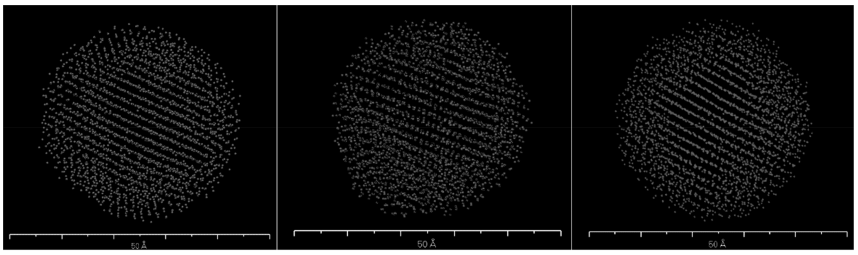

(a) 973 K (b) 1173 K (c) 1373 K

Figure 7. Structure and morphology of CuO clusters of 40 Å at different temperatures.

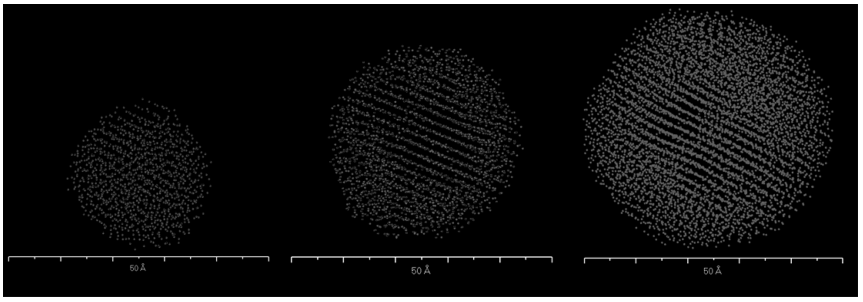

Figure 8. Structure and morphology of CuO clusters with different diameters at 1173 K.

characteristic of single CuO particle usually manifests a more irregular atom arrangement tendency along with the increase of operation temperature.

It can be seen in Figure 7 that the arrangement of internal atoms still maintains a fairly regular lattice arrangement at different temperatures. That is, from 973 to 1373 K, there is little effect of temperature on the lattice arrangement of internal atoms. However, the atomic disturbance of the surface layer is still strong. That says that the outer layer shows a "melting" state, while the inside maintains the "frozen" state. The degree of "melting" would be higher with the increase of temperature. On the basis of the above RDF analysis and particle morphology, it can be concluded that during the temperature range of CLOU, the internal lattice structure of copper oxide would change little, and the higher temperature only brings a small increase in the arrangement irregularity of the internal atoms.

Then, the structure difference of three kinds of particle size (30, 40, and 50 Å) at 1173 K was compared. As shown in Figure 6b, the RDF curve of bigger particle exhibits more and higher peaks, which can be explained by that the surface energy release process, driven by high temperature, exerting a more significant effect to the particles with smaller diameter. With the increase of particle size, the proportion of disturbed area will decrease, and more regular district is allowed to remain. This phenomenon can also be seen in the sintering of TiO_2 NPs.[19] In general, according to the high-temperature characteristics of single CuO grain, the change of size brings a large influence to the atomic configuration than thermodynamic condition. To compare the effect of particle size on the internal sintering structure, we simulated the structure and morphology of CuO clusters with different diameters at 1173 K. As shown in Figure 8, the arrangement irregularity of the internal atoms decreases as the CuO cluster diameter increases, which is also in accordance with the RDF results shown in Figure 6b.

3.2. High-Temperature Sintering Characteristics of Two CuO Grains. Furthermore, a simplified model consisting of two CuO NGs was built to investigate the coalescence properties of CuO NGs. Each particle contains 3344 atoms, with a diameter of 40 Å. Two CuO grains were separated by 5 Å first, then the system was equilibrated in the *NVT* ensemble at 1173 K with 1 000 000 time steps. Figure 9 gives the

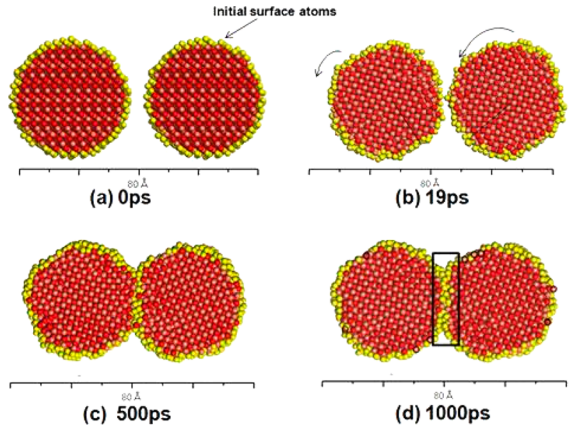

Figure 9. Snapshots of two CuO NGs sintering process at 1173 K for 0, 19, 500, and 1000 ps, and yellow atoms present initial surface atoms.

snapshots of two CuO NGs sintering processes at 0, 19, 500, and 1000 ps, respectively. In order to observe the diffusion of atoms during sintering process, the cross-section photos were shown and the initial surface atoms were marked by different color. At the beginning of simulation, two CuO NGs start to rotate counterclockwise spontaneously in the high temperature environment, adjusting the lattice planes to the most energetically favorable facet, which indicates the existence of a polar attraction between particles. This oriented attachment phenomenon has also been observed in the previous MD

DOI: 10.1021/acs.jpcc.8b04253
J. Phys. Chem. C 2018, 122, 25595−25605

simulation of TiO_2 sintering.[19] After 19 ps, the CuO NGs start to contact with each other gradually and a neck region is formed. During the growth process of neck region, surface atoms migrate to the contacted area while some subsurface atoms migrate to the outside (see Figure 9, parts c and d), which are marked with black circles in Figure 9d. Finally, many surface atoms accumulate in the neck region and a new regular lattice is formed in the middle part. However, when the initial surface atoms migrate toward the neck region, gaps appear on the surface of the cluster, and internal atoms near the gap begin to migrate outward and form a new surface layer, and finally the neck is continuously developed.

As is shown in Figure 9d, the arrangement of the atoms in the neck region tends to be in a regular lattice arrangement, which is unlike to its surface layer atoms. The enlarged view of the neck region is shown in Figure 10, where we can see that

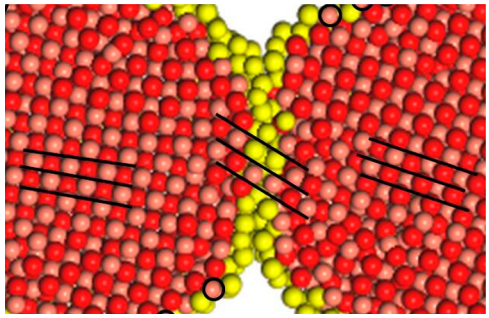

Figure 10. Partial enlarged view of the neck region in the sintering of two CuO NGs at 1000 ps.

the direction of crystal lattice is different from that inside particles. However, the lattice arrangement of this part is not uniform with the lattice order inside the two clusters. Factually, a phenomenon similar to lattice slip occurs, which is like the mechanism of shear transformations zone. It means that there is a new crystal lattice formed in the neck region. It is not like the arrangement of surface atoms, but exhibits a regular placement with lattice slip, which is difficult to observe via an optoelectronic technique.

Up to now, the diffusion mechanism during particle sintering includes the following: surface diffusion, grain boundary diffusion, volume diffusion, condensation and evaporation, and viscous flow diffusion.[37,38] On the one side, from the above snapshots of CuO sintering process, we can see that the thermal motion is not strong enough to lead condensation and evaporation and viscous flow diffusion during the sintering. On the other side, as known, the surface diffusion is driven by the excess surface energy; and the grain boundary diffusion is attributed to the uneven distribution of gaps in the atoms arranged in the neck after contact. The gap difference leads to the generation of stress on the grain boundary which causes the atoms to move along the grain boundaries. The grain boundary is formed inside the neck, and the surface atoms migrate to the outside with high surface energy. In the aggregation process of CuO pairs, numerous surface atoms diffuse to the bonding region, which is driven by the excess surface energy of surface atoms. Also, a significant grain-boundary is formed inside the neck region due to the high concentration of defects. Hence, one may deduce that the neck growth is the combined effect of surface diffusion (surface energy release) and grain boundary diffusion (shrinkage of centers).

To compare the diffusion of interior atoms and surface atoms during the simulation, the mean square displacement (MSD) of them was calculated with the following expression:

$$r^2(t) = \frac{1}{N}\sum_{i=0}^{N} |r_i(t) - r_i(0)|^2 \quad (4)$$

Here $r^2(t)$ is the MSD, N is the total number of diffusing atoms, and t is the time of the simulation, and $r_i(t)$ and $r_i(0)$ are the position at time t and that at initial time of an atom i, respectively.

Figure 11 indicates the mean square displacement (MSD) of both interior atoms and surface atoms experience fluctuation

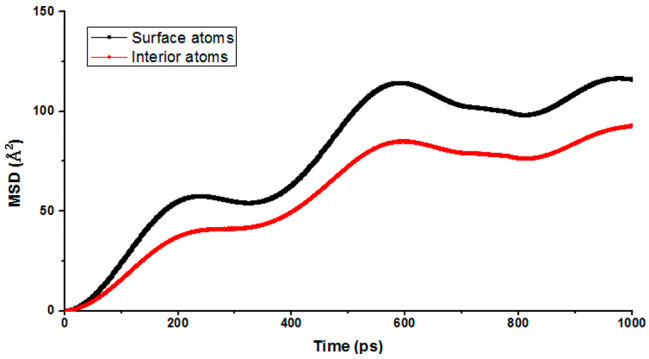

Figure 11. Mean square displacement of the initial surface atoms and the interior atoms.

over time. The MSD corresponds to the atom's diffusion coefficient, and is a three-dimensional variable. Although the surface atoms may not move along the radial direction, they may move violently along other two directions. So the value of the MSD shown in Figure 11 becomes larger. During the sintering process, the atom would leave its initial position, but it may move along any direction. As a result, the atoms gradually return to a new equilibrium state, and the MSD would go back and forth.

As seen in Figure 11, the MSD of the initial surface atoms is greater than that of the initial interior atoms. This indicates that the diffusion of surface atoms is more intensive than that of interior atoms. At the first 19 ps, the MSD of the atoms rises slowly as the particles rotate and approach to each other. When the contact of particles happens, the surface atoms diffuse and migrate to the neck region. This may cause the faster increase in MSD value of surface atoms and the increase of the MSD difference between the surface and interior atoms. The interior atoms behave like a solid, whereas the surface atoms remain liquid-like. When more and more initial surface atoms migrate to the neck region and become interior atoms in the neck region, the number of the initial surface atoms on the surface decreases, and the interior atoms tend to diffuse to the surface area and become surface-like. This may explain why the difference between the MSD values of the surface and interior atoms remains relative stable finally. According to this, surface diffusion should be the dominant mechanism in the sintering of CuO NGs, and it contributes to the formation of the grain boundary and the growth of the neck.

On the basis of the sintering mechanism analysis, the influences of temperature and particle size were studied

DOI: 10.1021/acs.jpcc.8b04253
J. Phys. Chem. C 2018, 122, 25595−25605

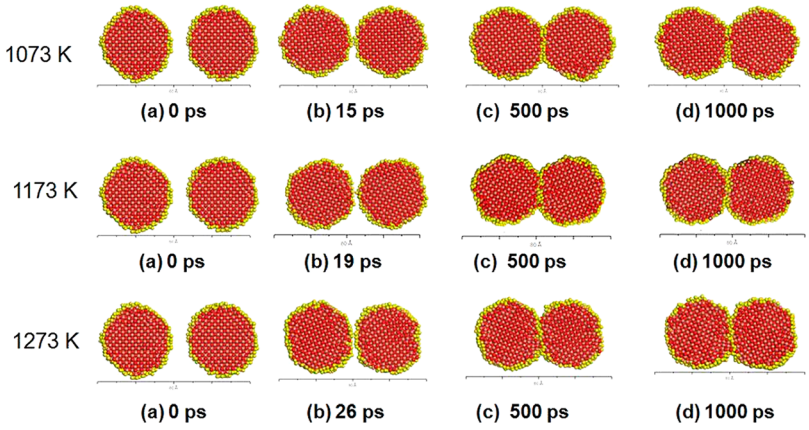

Figure 12. Snapshots of CuO pairs sintering processes at different temperatures.

separately. The sintering of OC particles commonly leads to a decrease of surface area, therefore it was calculated to judge the sintering degree here. The surface area changes as the function of simulation time was measured by the Meyer method,[39] and the simulation cell was divided into small mesh grids by a length of 0.1 Å. The grids within the van der Waals (VDW) radius were defined as NGs interior grids. The van der Waals radii for Cu and O are 2.16 and 1.52 Å respectively.[40] The grids in contact with the NG interior grids were defined as surface grids and used for calculating the surface area. The sintering processes at 1073, 1173, and 1273 K were captured and shown in Figure 12, while the corresponding surface loss is given by Figure 13.

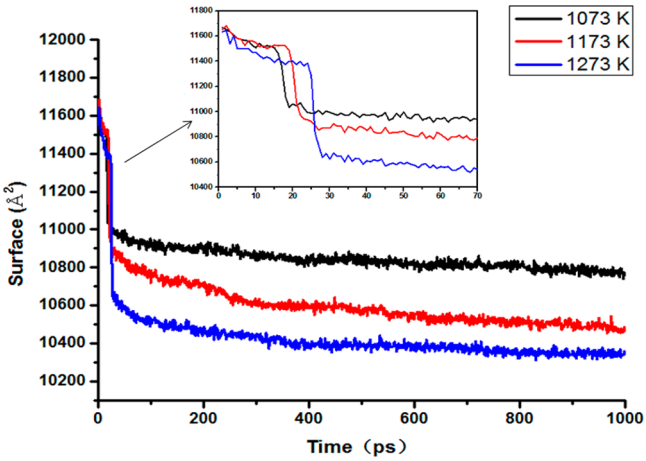

Figure 13. Time evolution of surface area for CuO pairs at 1073, 1173, and 1273 K.

From Figure 12, we can see that the sintering processes of CuO pairs at different temperature are very similar. First the rotation of two nanograins occurs to reach a force balance. Next, they contact to each other and start to form a neck region. Since atom motion is a completely random motion, the particle may not exactly exist in the middle of the scale. With the growth of the neck region, surface atoms migrate to the gap constantly. The arrangement of the interior atoms remains regular during sintering process. This implies that the sintering at these temperatures can not destroy the lattice oxygen in the CuO NGs. Furthermore, the CuO pairs at higher temperatures show more irregular atoms arrangement, which is consistent with the RDF result of single CuO NG sintering.

In Figure 13, at the initial stage, the surface areas show little change. Then a quickly decrease happens at 15, 19, and 26 ps for temperatures of 1073, 1173, and 1273 K, respectively, which corresponds with the moment of particles contact. Finally, the relative surface loss increases slowly and remains relative stable. The final surface loss at 1073, 1173, and 1273 K are 897.41, 1183.72, and 1280.81 Å^2. Thus, the higher temperature causes the deeper sintering degree, which is ascribed to that the increased thermal force intensifies the motion of atoms and agitates the diffusion to the neck. Interestingly, at a lower temperature two CuO nanograins consume less time to touch. This may be caused by the weaken Coulomb dipolar interactions at high temperature, which can also be seen in the sintering of TiO_2 NPs.[41]

The influence of particle size was investigated by heating a group of CuO particle with three different diameters (30, 40, and 50 Å) at 1173 K. The relative surface change of CuO pairs during the sintering process (as shown in Figure 14) was calculated as $k = S_t/S_0$, where S_0 is the initial surface before sintering, and S_t is the surface area at t ps. Similarly, the relative surface shows little variation at the initial stage, indicating that the particle surface remains stable before contacting with each other. Then a huge decrease in surface area appears at the

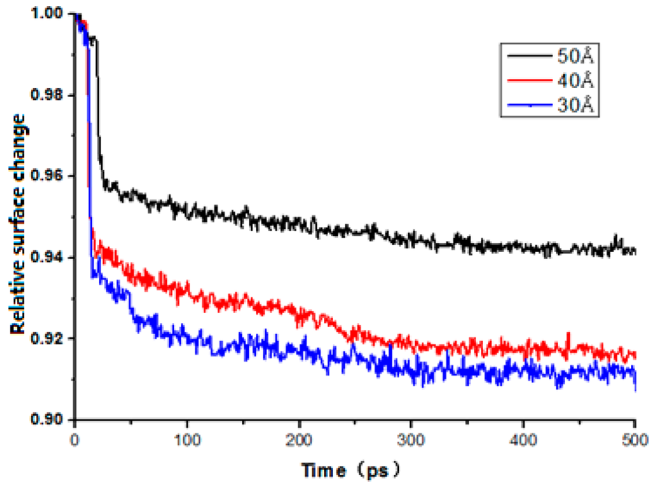

Figure 14. Time evolution of the relative surface area for CuO pairs with different diameters at 1173 K.

DOI: 10.1021/acs.jpcc.8b04253
J. Phys. Chem. C 2018, 122, 25595−25605

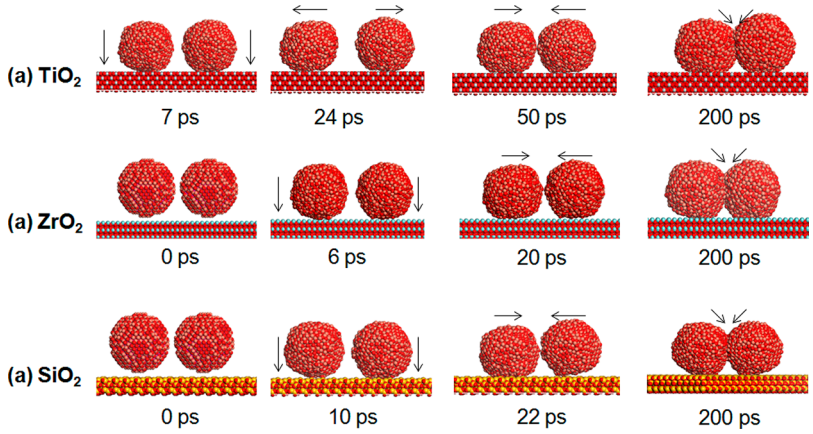

Figure 15. Snapshots of supported CuO pairs sintering processes at 1173 K: (a) CuO/TiO_2; (b) CuO/ZrO_2; (c) CuO/SiO_2.

contact moment. The eventual relative surface losses of CuO NGs with diameter of 30, 40, and 50 Å are 8.8%, 8.5%, and 5.8%, respectively. The bigger particles tend to have a smaller relative surface loss, which means the increase of diameter enhances the resistance to sintering. From the foregoing discussion of single particle structure and MSD of two particles sintering, we concluded that the surface diffusion is the dominant mechanism in sintering process of CuO NGs. Since the smaller particle has higher proportion of surface atoms, the diffusion between smaller particles will be more rapid and intensive. This can explain why the large particle shows higher resistance in sintering.

3.3. High-Temperature Sintering Characteristics of Supported CuO Grains. To study the effect of different support materials on the sintering of CuO OCs, simplified models consisting of two CuO NGs (40 Å) on the TiO_2 (110), ZrO_2 (100) and SiO_2 (110) surfaces were built separately. Before temperature coupling, the lattice orientation of these CuO particles were all arranged to the same: (010) plane to (010) plane. Then, all models were equilibrated in the *NVT* ensemble at a temperature of 1173 K with 200 000 time steps. The snapshots of the sintering of the CuO NGs on the TiO_2 (110), ZrO_2 (100) and SiO_2 (110) surfaces are shown in Figure 15.

Different from CuO/ZrO_2 and CuO/SiO_2 systems, the CuO NGs on TiO_2 (110) will separate from each other at first (as shown in Figure 15a). The possible reason for this special phenomenon might be that TiO_2 (110) slab has a strong effect on the Coulomb dipolar interaction between the CuO particles. As the Coulomb dipolar force of TiO_2 is much large than the VDW force at long-range distance,[42] the Coulomb field generated by TiO_2 slab would be responsible for the abnormal movement track of CuO particles. This kind of force would transform from repelling to attraction along with the adjustment of lattice orientation.

Here, the adsorption structures between active component and inert materials hinder the measurement of surface area. The alternative representing sintering degree is to detect the mass center distance. Figure 16 shows the time evolution of mass center distance between two CuO particles. At the first few picoseconds, CuO NGs go through a downward movement to bond with the support surfaces, the distance between the CuO particles decrease slowly and remain relative constant. Then, the CuO particles supported on ZrO_2 (100) or SiO_2 (110) surface start to approach to each other, driven by the Coulomb and VDW forces. However, the approaching

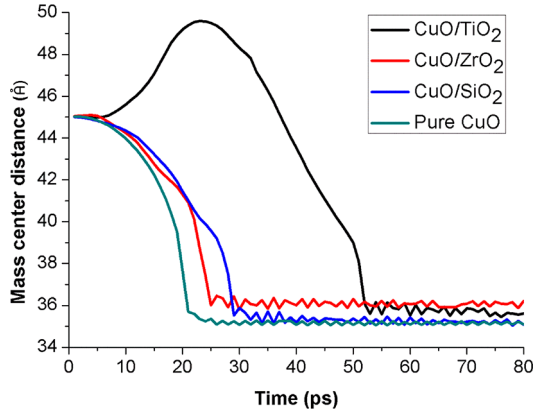

Figure 16. Time evolution of the mass center distance in CuO/TiO_2, CuO/ZrO_2, CuO/SiO_2, and CuO models at 1173 K.

speed of these supported CuO particles is slower than that of the unsupported CuO particles. It indicates that the pinning force generated by support surface reduces the attraction between CuO NGs. Finally, the mass center distance converges to a constant, 35.71, 36.01, and 34.97 Å for CuO/TiO_2, CuO/ZrO_2, and CuO/SiO_2, respectively.

The results displayed in Figure 16 suggest that ZrO_2 exhibits a better sintering resistance than TiO_2 and SiO_2. The curve of CuO/SiO_2 shows little difference from the pure CuO in sintering resistance and indicates that the addition of SiO_2 only plays a role of dispersant in oxygen carriers. From the whole sintering process, we can see that the high Coulomb long-range interaction only affects the sintering rate, yet it cannot determine the final sintering degree. The diffusion of Cu and O atoms after the contact will determine the sintering degree, which may mainly be affected by the short-range interaction.

For comparison, the sintering simulations of supported CuO NGs at different temperatures were performed, the same models of 40 Å CuO NGs on the TiO_2 (110), ZrO_2 (100) and SiO_2 (110) surface were heated to different temperatures of 1073 and 1273 K as well. The particle arrangement and the heating method are consistent with the above study of 1173 K, and the intuitional morphology evolution is given in Figure 17, Figure 18, respectively. We can see that the sintering of CuO NGs on different supported materials exhibits similar process. The particles first adjust the orientation of the atoms to find energetically favorable contacted points. Then the particles contact and diffuse to each other. With the migration of the

DOI: 10.1021/acs.jpcc.8b04253
J. Phys. Chem. C 2018, 122, 25595−25605

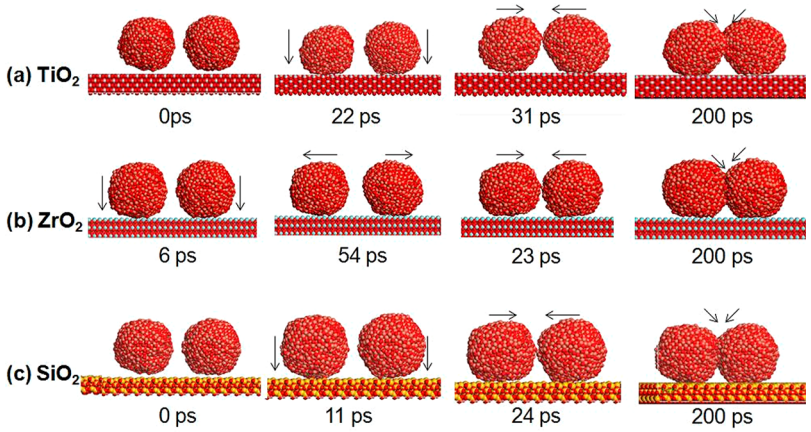

Figure 17. Snapshots of the sintering process of CuO NGs at 1073 K: (a) CuO/TiO_2; (b) CuO/ZrO_2; (c) CuO/SiO_2.

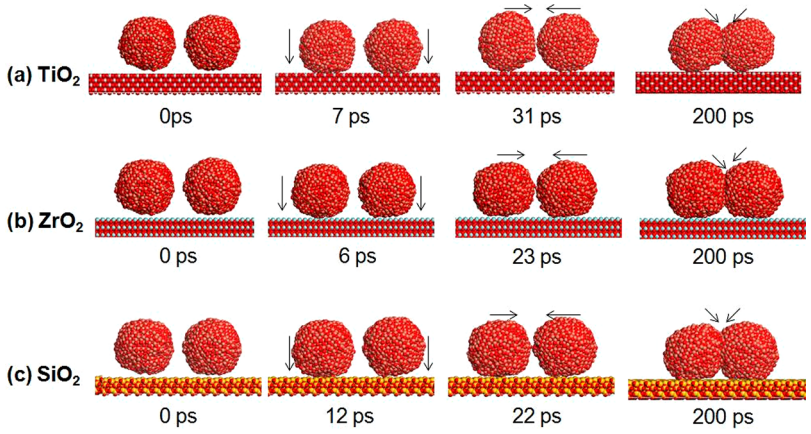

Figure 18. Snapshots of the sintering process of CuO NGs at 1273 K: (a) CuO/TiO_2; (b) CuO/ZrO_2; (c) CuO/SiO_2.

atoms, the neck region grows constantly. The abnormal separation in the ZrO_2 case at 54 ps in Figure 17b is similar to that in the TiO_2 case at 24 ps (Figure 15a). Figure 19 shows the time evolution of the mass center distance of the CuO particles, which are supported on the TiO_2 (110), ZrO_2 (100), and SiO_2 (110) surface at three different temperatures.

The final distance at 1273 K is obviously shorter than that of 1073 K for all three supported CuO particles while the temperature rise from 1073 to 1173 K poses less impact on the sintering degree. This may means that when the inner temperature of these kinds of OC reaches 1273 K, there will be an irreversible destruction to the active components. Besides, the CuO/ZrO_2 always show the best sintering resistance at all temperature conditions. And the interaction between CuO and SiO_2 might be too weak to withstand the thermal force. As can be found in Figure 19, the discrepancy of final distance becomes large with the increase of temperature, which emphasizes the importance of rational selection of support materials at high temperatures.

4. CONCLUSIONS

The oxygen carrier (OC) based on copper oxide always faces the sintering problem, and many support materials are applied to improve the stability of OCs. This work investigated the microscopic sintering properties of CuO nanograins (NGs) using the molecular dynamics (MD) simulations. The MD simulation of two unsupported CuO NGs shows that the migration of surface atoms forms the neck region between the particles, while some subsurface atoms migrate to the outside. From the analysis of neck region growth process, we may conclude that the neck growth of CuO sintering is the combined effect of surface diffusion and grain boundary diffusion. The surface area loss when two CuO NGs sinter at different temperatures with different diameters was detected. On the one hand, the particle pairs at a higher temperature take more time to contact with each other, but the higher temperature would finally cause a deeper sintering degree. It is interpreted as that the effect of Coulomb dipolar attraction limits the final sintering degree. On the other hand, the larger particle shows higher resistance in sintering. This is because the smaller particles have higher proportion of surface atoms, and the diffusion between smaller particles will be more rapid and intensive.

The CuO supported by ZrO_2 slab always shows better sintering resistance. The CuO particle supported by SiO_2 slab tends to have no difference from the unsupported CuO in sintering resistance, which indicates that the adsorption of SiO_2 slab is very weak and the SiO_2 may only play the role of dispersant in the CuO OC. When the temperature is elevated to 1273 K, the sintering degree of these supported CuO increased dramatically. The large discrepancy of final distance emphasizes the importance of rational selection of support materials at high temperature.

This study would be helpful for understanding of the microscopic sintering mechanism in Cu-based OCs. However, it should be mentioned that the real sintering process would be

DOI: 10.1021/acs.jpcc.8b04253
J. Phys. Chem. C 2018, 122, 25595−25605

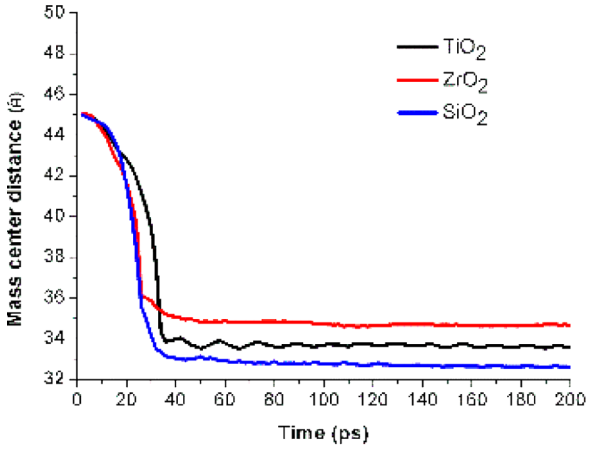

(a) 1273 K

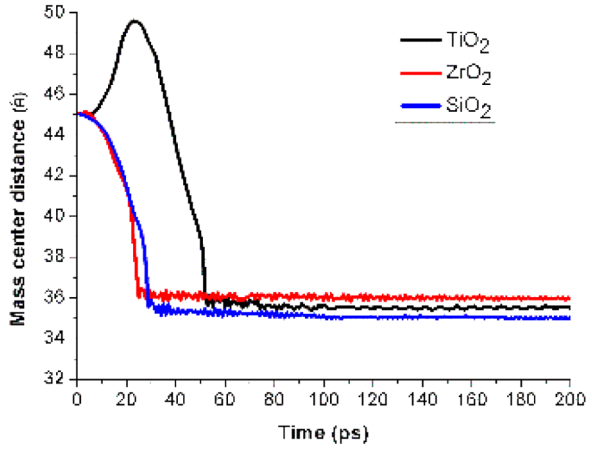

(b) 1173 K

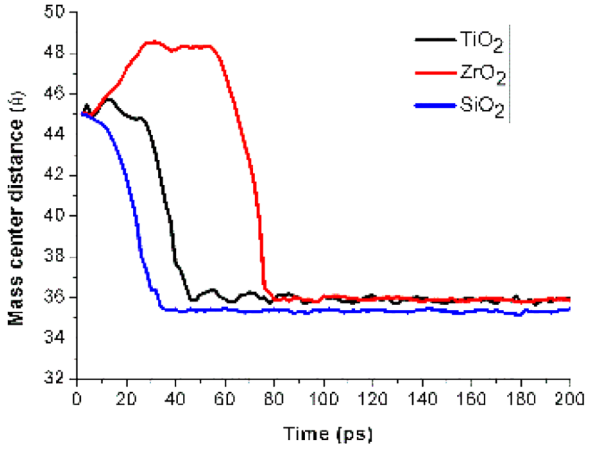

(c) 1073 K.

Figure 19. Time evolution of the mass center distance of the varieties supported CuO particles.

more complex, as the preparation process at high temperature will also affect the dispersion and migration of CuO. Furthermore, the sintering process of Cu_2O should be considered, since it also exists in a real oxygen carrier in a sizable amount.

AUTHOR INFORMATION

Corresponding Author

*(H.Z.) Telephone: +86 27 8754 4779 x8208. Fax: +86 27 8754 5526. E-mail: hzhao@mail.hust.edu.cn.

ORCID

Haibo Zhao: 0000-0002-2693-4499

Notes

The authors declare no competing financial interest.

ACKNOWLEDGMENTS

The authors were supported by the National Key R&D Program of China (2016YFB0600801) and National Science of China (51522603 and 51561125001).

REFERENCES

(1) Liang, X.; Reiner, D.; Li, J. Perceptions of Opinion Leaders Towards CCS Demonstration Projects in China. *Appl. Energy* **2011**, *88*, 1873−1885.

(2) Adanez, J.; Abad, A.; Garcia-Labiano, F.; Gayan, P.; de Diego, L. F. Progress in Chemical-Looping Combustion and Reforming Technologies. *Prog. Energy Combust. Sci.* **2012**, *38*, 215−282.

(3) Mattisson, T.; Lyngfelt, A.; Leion, H. Chemical-Looping with Oxygen Uncoupling for Combustion of Solid Fuels. *Int. J. Greenhouse Gas Control* **2009**, *3*, 11−19.

(4) Gayán, P.; Adánez-Rubio, I.; Abad, A.; de Diego, L. F.; García-Labiano, F.; Adánez, J. Development of Cu-Based Oxygen Carriers for Chemical-Looping with Oxygen Uncoupling (CLOU) Process. *Fuel* **2012**, *96*, 226−238.

(5) Imtiaz, Q.; Hosseini, D.; Müller, C. R. Review of Oxygen Carriers for Chemical Looping with Oxygen Uncoupling (CLOU): Thermodynamics, Material Development, and Synthesis. *Energy Technology* **2013**, *1*, 633−647.

(6) Sahir, A. H.; Sohn, H. Y.; Leion, H.; Lighty, J. A. S. Rate Analysis of Chemical-Looping with Oxygen Uncoupling (CLOU) for Solid Fuels. *Energy Fuels* **2012**, *26*, 4395−4404.

(7) Adánez-Rubio, I. a.; Arjmand, M.; Leion, H.; Gayán, P.; Abad, A.; Mattisson, T.; Lyngfelt, A. Investigation of Combined Supports for Cu-Based Oxygen Carriers for Chemical-Looping with Oxygen Uncoupling (CLOU). *Energy Fuels* **2013**, *27*, 3918−3927.

(8) Guo, L.; Zhao, H.; Wang, K.; Mei, D.; Ma, Z.; Zheng, C. Reduction Kinetics Analysis of Sol-Gel-Derived $CuO/CuAl_2O_4$ Oxygen Carrier for Chemical Looping with Oxygen Uncoupling. *J. Therm. Anal. Calorim.* **2016**, *123*, 745−756.

(9) Wang, B.; Zhao, H.; Zheng, Y.; Liu, Z.; Zheng, C. Chemical Looping Combustion of Petroleum Coke with $CuFe_2O_4$ as Oxygen Carrier. *Chem. Eng. Technol.* **2013**, *36*, 1488−1495.

(10) Zhao, H.; Mei, D.; Ma, J.; Zheng, C. Comparison of Preparation Methods for Iron−Alumina Oxygen Carrier and Its Reduction Kinetics with Hydrogen in Chemical Looping Combustion. *Asia-Pac. J. Chem. Eng.* **2014**, *9*, 610−622.

(11) Gayán, P.; Forero, C. R.; Abad, A.; de Diego, L. F.; García-Labiano, F.; Adánez, J. Effect of Support on the Behavior of Cu-Based Oxygen Carriers During Long-Term CLC Operation at Temperatures above 1073 K. *Energy Fuels* **2011**, *25*, 1316−1326.

(12) Smith, C. S. Grains, Phases, and Interfaces:An Introduction of Microstructure. *Trans. Metall. Soc. AIME* **1948**, *175*, 15−51.

(13) Li, Z.; Liu, Y.; Cai, N. Understanding the Effect of Inert Support on the Reactivity Stabilization for Synthetic Calcium Based Sorbents. *Chem. Eng. Sci.* **2013**, *89*, 235−243.

(14) Xu, L.; Wang, J.; Li, Z.; Cai, N. Experimental Study of Cement-Supported CuO Oxygen Carriers in Chemical Looping with Oxygen Uncoupling (CLOU). *Energy Fuels* **2013**, *27*, 1522−1530.

(15) Manohar, P. A.; Ferry, M.; Chandra, T. Five Decades of the Zener Equation. *ISIJ Int.* **1998**, *38*, 913−924.

DOI: 10.1021/acs.jpcc.8b04253
J. Phys. Chem. C 2018, 122, 25595−25605

(16) Zhao, H.; Zhang, Y.; Wei, Y.; Gui, J. Understanding CuO-Support Interaction in Cu-Based Oxygen Carriers at a Microcosmic Level. *Proc. Combust. Inst.* **2017**, *36*, 4069−4077.
(17) Schweigert, I. V.; Lehtinen, K. E.; Carrier, M. J.; Zachariah, M. R. Structure and Properties of Silica Nanoclusters at High Temperatures. *Phys. Rev. B: Condens. Matter Mater. Phys.* **2002**, *65*, 121.
(18) Zhang, H.; Chen, B.; Banfield, J. F.; et al. Atomic Structure of Nanometer-Sized Amorphous TiO_2. *Phys. Rev. B: Condens. Matter Mater. Phys.* **2008**, *78*, 214106.
(19) Buesser, B.; Gröhn, A. J.; Pratsinis, S. E. Sintering Rate and Mechanism of TiO_2 Nanoparticles by Molecular Dynamics. *J. Phys. Chem. C* **2011**, *115*, 11030−11035.
(20) Li, Y.; Kalia, R. K.; Nakano, A.; Vashishta, P. Size Effect on the Oxidation of Aluminum Nanoparticle: Multimillion-Atom Reactive Molecular Dynamics Simulations. *J. Appl. Phys.* **2013**, *114*, 134312.
(21) Ahmed, A.; Elvati, P.; Violi, A. Size-and Phase-Dependent Structure of Copper (Ii) Oxide Nanoparticles. *RSC Adv.* **2015**, *5*, 35033−35041.
(22) Xu, J.; Sakanoi, R.; Higuchi, Y.; Ozawa, N.; Sato, K.; Hashida, T.; Kubo, M. Molecular Dynamics Simulation of Ni Nanoparticles Sintering Process in Ni/YSZ Multi-Nanoparticle System. *J. Phys. Chem. C* **2013**, *117*, 9663−9672.
(23) Iskandarov, A. M.; Ding, Y.; Umeno, Y. Effect of Cation Dopants in Zirconia on Interfacial Properties in Nickel/Zirconia Systems: An Atomistic Modeling Study. *J. Phys.: Condens. Matter* **2017**, *29*, 045001.
(24) Diaz, R.; Guo, Z. A Molecular Dynamics Study of Phobic/Philic Nano-Patterning on Pool Boiling Heat Transfer. *Heat Mass Transfer* **2017**, *53*, 1061.
(25) Zeng, J.; Ma, X.; Zhu, Z.; Hou, Y.; Shi, W.; Bai, Y. Molecular Dynamics Simulation of the Interaction between Methyl Benzotriazole and Cu_2O Crystal. *Surf. Interface Anal.* **2017**, *49*, 1153−1159.
(26) Braga, C.; Travis, K. P. A Configurational Temperature Nose-Hoover Thermostat. *J. Chem. Phys.* **2005**, *123*, 134101.
(27) Miller, T.; Krogan, N. J.; Dover, J.; Erdjumentbromage, H.; Tempst, P.; Johnston, M.; Greenblatt, J. F.; Shilatifard, A. Compass: A Complex of Proteins Associated with a Trithorax-Related Set Domain Protein. *Proc. Natl. Acad. Sci. U. S. A.* **2001**, *98*, 12902−12907.
(28) Zhao, L.; Liu, L.; Sun, H. Semi-Ionic Model for Metal Oxides and Their Interfaces with Organic Molecules. *J. Phys. Chem. C* **2007**, *111*, 10610−10617.
(29) Yu, W.; Wu, L.; Shen, S. Adhesion Properties of Cu(111)/A-Quartz (0001) Interfaces: A Molecular Dynamics Study. *Mater. Sci. Eng., A* **2017**, *695*, 239−248.
(30) Liu, S.; Li, H.; He, Y.; Li, X.; Li, Y.; Wang, X. Pathway into the Silicon Nucleation on Silicene Substrate at Nanoscale. *Mater. Des.* **2015**, *85*, 60−66.
(31) Reed, A. E.; Curtiss, L. A.; Weinhold, F. Intermolecular Interactions from a Natural Bond Orbital, Donor-Acceptor Viewpoint. *Chem. Rev.* **1988**, *88*, 899−926.
(32) Zhang, Y.; Zhao, H.; Guo, L.; Zheng, C. Decomposition Mechanisms of Cu-Based Oxygen Carriers for Chemical Looping with Oxygen Uncoupling Based on Density Functional Theory Calculations. *Combust. Flame* **2015**, *162*, 1265−1274.
(33) Ghijsen, J.; Tjeng, L. H.; Van Elp, J.; Eskes, H.; Westerink, J.; Sawatzky, G. A.; Czyzyk, M. T. Electronic Structure of Cu_2O and CuO. *Phys. Rev. B: Condens. Matter Mater. Phys.* **1988**, *38*, 11322.
(34) Diebold, U. The Surface Science of Titanium Dioxide. *Surf. Sci. Rep.* **2003**, *48*, 53−229.
(35) Howard, C. J.; Hill, R. J.; Reichert, B. E. Structures of ZrO_2 Polymorphs at Room Temperature by High-Resolution Neutron Powder Diffraction. *Acta Crystallogr., Sect. B: Struct. Sci.* **1988**, *44*, 116−120.
(36) Weidner, D. J. Structure and Elastic Properties of Quartz at Pressure. *Am. Mineral.* **1980**, *65*, 920−930.
(37) Herring, C. Effect of Change of Scale on Sintering Phenomena. *J. Appl. Phys.* **1950**, *21*, 301−303.
(38) Kingery, W. D.; Berg, M. Study of the Initial Stages of Sintering Solids by Viscous Flow, Evaporation-Condensation, and Self-Diffusion. *J. Appl. Phys.* **1955**, *26*, 1205−1212.
(39) Meyer, A. Y. Molecular Mechanics and Molecular Shape. V. On the Computation of the Bare Surface Area of Molecules. *J. Comput. Chem.* **1988**, *9*, 18−24.
(40) Batsanov, S. S. Van Der Waals Radii of Elements. *Inorg. Mater.* **2001**, *37*, 871−885.
(41) Zhang, Y.; Li, S.; Yan, W.; Yao, Q.; Tse, S. D. Role of Dipole-Dipole Interaction on Enhancing Brownian Coagulation of Charge-Neutral Nanoparticles in the Free Molecular Regime. *J. Chem. Phys.* **2011**, *134*, 084501.
(42) Yan, W.; Li, S.; Zhang, Y.; Yao, Q.; Tse, S. D. Effects of Dipole Moment and Temperature on the Interaction Dynamics of Titania Nanoparticles During Agglomeration. *J. Phys. Chem. C* **2010**, *114*, 10755−10760.

DOI: 10.1021/acs.jpcc.8b04253
J. Phys. Chem. C 2018, 122, 25595−25605